Title

Metal-Templated Design of Chemically Switchable Protein Assemblies with High-Affinity Coordination Sites

Journal

Angewandte Chemie International Edition, 59(49)

ISSN

1433-7851

Authors

Kakkis, Albert
Gagnon, Derek
Esselborn, Julian
et al.

Publication Date

2020-12-01

DOI

10.1002/anie.202009226

Peer reviewed

HHS Public Access

Author manuscript

Angew Chem Int Ed Engl. Author manuscript; available in PMC 2021 June 01.

Published in final edited form as:

Angew Chem Int Ed Engl. 2020 December 01; 59(49): 21940–21944. doi:10.1002/anie.202009226.

Metal-Templated Design of Chemically Switchable Protein Assemblies with High-Affinity Coordination Sites

Albert Kakkis[a], **Derek Gagnon**[a], **Julian Esselborn**[a], **R. David Britt**[b], **F. Akif Tezcan**[a]

[a]Department of Chemistry and Biochemistry, University of California, San Diego, 9500 Gilman Drive, La Jolla, CA 92093 (USA)

[b]Department of Chemistry, University of California, Davis, 1 Shields Avenue, Davis, CA 95616 (USA)

Abstract

To mimic a hypothetical pathway for protein evolution, we previously developed a design strategy (Metal-Templated Interface Redesign), in which a monomeric protein (cytochrome cb_{562}) was tailored for metal-mediated self-assembly, followed by the re-design of the resulting oligomers for enhanced stability and metal-based functions. Here we show that a single hydrophobic mutation on the cytochrome cb_{562} surface can drastically alter the outcome of metal-directed oligomerization to yield a new trimeric architecture, $(TriCyt1)_3$, featuring an unusual hexa-histidine coordination motif. Through computational and rational redesign, this nascent trimer is converted into second and third-generation variants $(TriCyt2)_3$ and $(TriCyt3)_3$ with increased structural stability and preorganization for metal coordination. The three TriCyt variants combined furnish a unique design platform to a) provide tunable coupling between protein quaternary structure and metal coordination, b) enable the construction of metal/pH-switchable protein oligomerization motifs, and c) generate a robust metal coordination site that can accommodate all mid-to-late first-row transition metal ions with high affinity, including Mn(II) with nanomolar dissociation constants, rivaling those of the strongest Mn(II)-binding protein, calprotectin.

Graphical Abstract

tezcan@ucsd.edu.

Supporting information for this article is given via a link at the end of the document.

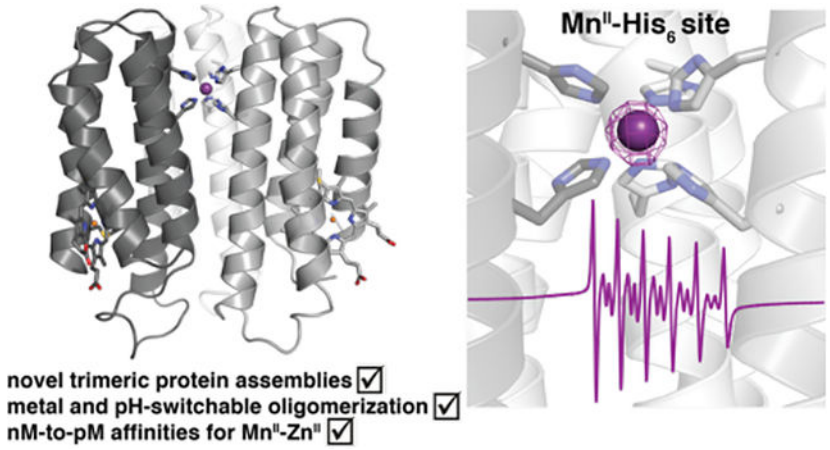

A metal-template-based protein design strategy is used to generate a series of trimeric protein assemblies with chemically tunable self-assembly properties and a rare hexa-histidine coordination motif that can accommodate all mid-to-late first-row transition metal ions with high affinity, including Mn(II) with nanomolar dissociation constants.

Keywords

Bioinorganic Chemistry; EPR spectroscopy; Metalloproteins; Protein design; Protein structures; Supramolecular Chemistry

Metalloproteins perform countless biological functions despite the fact that they co-opt barely more than a handful of transition metal ions.[1] Underlying this functional diversity is a complex interplay between metal coordination/reactivity and protein structure/dynamics.[2] Although the metal-protein interplay can often be understood through detailed, top-down studies of natural metalloproteins,[3] it remains considerably more challenging to build this interplay from scratch in the form of new metalloproteins.[4] Starting with pioneering studies in the 1990's,[5] there have been notable successes in the de novo design of functional metalloproteins,[6] which are predominantly based on four-helix bundle and α-helical coiled-coiled motifs with readily parametrizable structures.[7] On the one hand, the fact that diverse bioinorganic functions can be obtained only with a limited set of structural motifs illustrates the versatility of the *de novo* design approach. On the other hand, it also highlights the challenge of – and the need for – devising alternative strategies and designing new protein architectures for building bioinorganic complexity in a bottom-up fashion.

It has been hypothesized that some modern metalloproteins may have emerged through the metal-nucleated oligomerization of small peptides or protein domains, followed by the evolution of the resulting assemblies into stable, functional architectures.[8] Based on this hypothetical trajectory, we previously developed a protein design strategy termed Metal-Templated Interface Redesign (MeTIR),[9] primarily using a monomeric, four-helix bundle protein (cytochrome cb_{562}) as a building block.[10] First, we installed two bis-His motifs (H59/H63, H73/H77) on the Helix3 surface of cyt cb_{562} to enable metal coordination.[11] The resulting construct, MBPC1, assembled into different oligomeric states depending on

the coordination preferences of nucleating metal ions (Ni^{II}-trimer; Cu^{II}-dimer; Zn^{II}-tetramer) (Figure S1).[11–12] Given the extensive protein-protein interfaces in the D_2 symmetric Zn_4:$MBPC1_4$ tetramer, this assembly was chosen as a platform for MeTIR.[9a] Zn_4:$MBPC1_4$ was elaborated through rational redesign and directed-evolution to build functional architectures that selectively bound metal ions,[13] displayed allostery,[14] and performed catalytic reactions *in vivo*.[15] Yet, despite the functional versatility of the Zn_4:$MBPC1_4$ progeny, they are inherently biased by the metal-templating strategy toward Zn^{II} coordination chemistry. Moreover, because of their D_2 symmetry, they possess at least four copies of each metal center of interest, complicating the examination and modification of the individual metal centers.

Here we aimed to direct the self-assembly of MBPC1 toward more pre-organized architectures in lower oligomerization states, possibly with fewer metal centers. It is well-established that surface-exposed hydrophobic residues can effectively induce protein-protein interactions and aggregation.[16] Thus, we incorporated a Trp residue (W70) onto the MBPC1 Helix3 surface between the H59/H63 and H73/H77 motifs to enable the formation of a hydrophobic core upon metal-mediated oligomerization (Figure 1a and S1). We also mutated the negatively charged Asp66 sidechain on the same surface to Asn to avoid repulsive electrostatic interactions during self-assembly.

The metal-dependent assembly of the resulting variant, TriCyt1, was first screened by crystallization in the presence of one equivalent (3 mM) of all mid-to-late first-row transition metal ions (Mn^{II} to Zn^{II}). Regardless of the metal ion identity, we observed crystals with hexagonal morphologies, suggesting that they shared an underlying protein arrangement with three-fold symmetry. We obtained 2.5-Å resolution crystal structures of the Ni^{II}- and Cu^{II}-TriCyt1 complexes (Figure 1b and S2). These structures revealed isostructural trigonal (*P*321) lattices, formed by trimeric TriCyt1 substructures containing a single Ni^{II} or Cu^{II} ion coordinated in a near-octahedral geometry by three pairs of H73/H77 residues. The trimeric substructures feature a closepacked, parallel arrangement of TriCyt1 monomers. Near the center is a hub of T-stacked W70 sidechains that non-covalently buttress the metal-coordinating H73 residues (Figure 1b and S3). Additionally, there are three pairs of intermonomer, salt-bridging interactions between R34 and D74 residues that surround the metal coordination site and the tris-W70 hub. The D74 carboxylates are further H-bonded to the δ-N's of H73 imidazoles from the same monomer, thus completing an extensive network of interactions surrounding the metal coordination site (Figure 1b). Interestingly, H59/H63 pairs are not coordinated by metal ions.

Collectively, these structural details suggested that the crystallographically observed trimeric TriCyt1 structure possesses a high degree of preorganization, which allows it to accommodate only a single metal ion within the same His_6 coordination motif independently of the metal identity. Indeed, analytical ultracentrifugation (AUC) and size-exclusion chromatography (SEC) experiments showed that TriCyt1 was monomeric in solution, but exclusively formed trimers upon addition of one equiv. of Mn^{II}, Fe^{II}, Co^{II}, Ni^{II}, Cu^{II} and Zn^{II} (Figure 1c and S4–S5). The yield of trimer formation in solution roughly followed the Irving-Williams series,[1c, 17] ranging from 12% for Mn^{II} to ~95% for Co^{II} (Figure 1c and S4).

Metal coordination by a His_6 motif is exceedingly rare in bioinorganic chemistry. The only well-established biological example is found in the immune protein calprotectin,[18] which is involved in the sequestration of metal ions (particularly Mn^{II}) to limit microbial growth and boasts one of the highest Mn^{II} affinities among natural proteins.[19] Given the rarity of the His_6 motif, in addition to the challenge of generating stable Mn coordination sites in proteins, we asked whether the TriCyt1 structure could be subjected to MeTIR to design progressively more stable trimers, which can subsequently bind Mn^{II} (and other divalent ions) with high affinity. The M^{II}:$(TriCyt1)_3$ trimer presents extensive intermonomer interactions (>3000 $Å^2$), which are dominated by a central interface formed by Helices3 of the monomers and peripheral interfaces between neighboring Helices2 and 3 (Figure 1b). We first undertook a computational redesign of these interfaces, whereby the “core motif” (His_6 site + tris-W70 hub + R34/D74 salt-bridges) and the protein backbone positions were maintained. Through an iterative process involving sidechain and rotamer optimization with Rosetta and visual inspection, we generated the second-generation variant, TriCyt2, which includes six additional surface mutations on TriCyt1. AUC and SEC experiments showed that TriCyt2 was stable and monomeric in solution but now trimerized in near-quantitative yield upon binding Mn^{II} (as well as the other tested metal ions) (Figure 2a and S4–5). Notably, this represents an 8-fold improvement in Mn^{II}-induced oligomerization.

These observations indicate that interface redesign was successful and furnished a unique protein construct that can conditionally assemble into trimers in the presence of all relevant first-row transition metal ions. We determined the 1.7-Å-resolution crystal structure of Fe^{II}-bound TriCyt2 complex, which is nearly isostructural with M^{II}:$(TriCyt1)_3$ complexes (rmsd = 0.86 Å over all 318 α-C’s) (Figure 2b). As designed, the H59I, H63V, V69L mutations contribute to hydrophobic packing in the Helix3 central core while eliminating the non-coordinating H59/H63 motif, whereas the Q41K and N66D substitutions generate a closed network of H-bonding interactions in the same core (Figure 2c). Additionally, the D54A mutation eliminates the potential repulsive interactions between the Asp54 chains, which causes a slight compaction of the trimer near the 50’s loops (Figure S6). In combination, the six designed mutations yield an increase in sidechain packing in the TriCyt2 trimer interior (buried surface area or BSA = 3440 $Å^2$) compared to TriCyt1 (BSA = 3050 $Å^2$) (Figure S7), consistent with increased trimer stability. Notably, TriCyt2 forms a trimer in the crystal lattice even in the absence of metal ions, revealing an essentially identical structure (rmsd = 0.37 Å) to the Fe^{II}:$(TriCyt2)_3$ complex that includes a pre-organized His_6 site (Figure S8).

In the next stage of redesign, we sought to stabilize the peripheral interfaces between Helices2 and 3 from neighboring monomers to obtain a metal-independent trimer in solution. Although the peripheral interfaces are wider and less packed compared to the central interface, they appeared amenable to engineering complementary electrostatic interactions. Accordingly, we incorporated three Lys (T31K, A35K, N80K) and two Glu (I67E, Q71E) residues into TriCyt2. The resulting third-generation variant, TriCyt3, indeed formed trimers even in the absence of metal ions (Figure 3a). Consistent with their electrostatic stabilization, TriCyt3 trimers reversibly dissociate into monomers upon lowering the solution pH to <4 (likely due to protonation of Glu/Asp residues), even in the presence of tightly binding metal ions such as Cu^{II} (Figure S9), thus providing a pH-switchable protein assembly platform. We determined the TriCyt3 trimer structure in

complex with Mn^{II}, Co^{II}, Ni^{II} and Cu^{II} ions (resolutions ranging from 1.8 to 2.2 Å), which showed little deviation from the TriCyt2 trimers (overall rmsd = 0.37 Å) (Figure 3b and S10). The redesigned peripheral interfaces exhibit increased electrostatic complementarity, owing largely to a network of H-bonding/electrostatic interactions involving the Lys and Glu residues (Figure 3b and Figure S11). An examination of metal coordination in the four M^{II}:$(TriCyt3)_3$ structures point to a stable His_6 site that can accommodate all tested metal ions in near-octahedral geometries (Figures 3c and S12). Of particular note is the unusual Cu^{II}-His_6 coordination, which has–to the best of our knowledge–not been previously observed in a protein scaffold and highlights the ability of the TriCyt3 scaffold to enforce a hexacoordinate geometry. Electron paramagnetic resonance (EPR) spectra of Mn-, Co- and Cu-TriCyt3 complexes are all consistent with metal centers in +2 oxidation states (Figures 4a and S16). Despite the enforcement of His_6 binding by the TriCyt3 scaffold, there appears to be some flexibility in metal coordination, as evidenced by a) the relatively high temperature factors of the H77 residues in all structures, b) the observation of both Λ and Δ isomers for the Co^{II}-His_6 species (Figure S12), and c) varying extents of deviation of the coordination bond angles from perfect octahedral geometry among different metal centers (Figure S13).

Having uncoupled protein oligomerization from metal binding, we measured the metal binding affinities of $(TriCyt3)_3$ via competitive titrations, using Mag-Fura-2 and Fura-2 as chelating indicators.[13c, 20] All titrations were consistent with one M^{II}/one trimer stoichiometry, yielding dissociation constants (K_d) ranging from 50 nM for Mn^{II} to <1 pM for Cu^{II} (Figures 4b, 4c and S14–15). The Mn^{II} affinity is noteworthy as it approximates the lowest K_d's reported for the Mn-His_6 center of calprotectin (which range from low nM to low μM)[19] and is >1000-fold lower than that for the Mn-regulatory protein, MntR (K_d = 50–160 μM)[21] and >14-fold lower than that for a designed protein with the highest reported Mn^{II}-binding affinity (K_d = 700 nM).[22] Despite the apparent crystallographic disorder in H77 positions, the X-band EPR spectrum of Mn^{II}:$(TriCyt3)_3$ (Figure 4a) is very similar to that of the His_6-Mn^{II} site in calprotectin.[18a] The zero-field splitting of Mn^{II}:$(TriCyt3)_3$ (300 MHz; E/D = 0.30) is in fact lower than that of Mn^{II}-calprotectin (485 MHz; E/D = 0.30), consistent with a highly symmetrical coordination environment.

In summary, we have reported here the metal-templated design of a series of trimeric protein assemblies (TriCyt1–3), which a) provide tunable coupling between protein quaternary structure and metal coordination, b) furnish metal/pH-switchable protein oligomerization motifs, and c) enable the construction of a robust coordination site for all mid-to-late first-row transition metal ions, including the highest Mn^{II} affinities achieved in an artificial protein. From a practical standpoint, the TriCyt platform offers important advantages for the bottom-up design of functional metalloproteins. Owing to its construction from cytochrome cb_{562} monomers (rather than peptide chains), it is stable and structurally tractable. At the same time, it enables the metal centers to be built in extensive, evolutionarily-naïve interfaces that can be liberally modified to tune the metal-protein interplay and protein oligomerization without affecting protein stability (which stands in contrast to *de novo* designed α-helical metalloproteins).[7] This could, among other possibilities, enable systematic investigations of the redox properties of the unusual Cu-His_6 (and likely also Fe-His_6) coordination motif, as well as the design of coordinatively unsaturated metal centers with potential chemical reactivities. From an evolutionary standpoint, our findings illustrate

that even a single mutation on a protein's surface (e.g., W70) can divert protein self-assembly into drastically different pathways, in turn leading to the emergence of new structural motifs with nascent functional sites in protein-protein interfaces.

Supplementary Material

Refer to Web version on PubMed Central for supplementary material.

Acknowledgements

We thank R. Subramanian and T. Choi for helpful discussions. This work was funded by the NSF (CHE1607145), by the NIH (a CBI traineeship to A.K. through T32GM112584 and R01GM138884 to F.A.T), by NASA (80NSSC18M0093; ENIGMA: Evolution of Nanomachines in Geospheres and Microbial Ancestors (NASA Astrobiology Institute Cycle 8)). Portions of this research were carried out at the Stanford Synchrotron Radiation Lightsource at the Stanford Linear Accelerator Center and the Advanced Light Source at the Lawrence Berkeley National Laboratory, which are supported by the DOE, Office of Science, Office of Basic Energy Sciences under contracts DE-AC02-76SF00515 and DE-AC02-05CH11231, respectively. Coordinate and structure factor files for the crystal structures have been deposited into the Protein Data Bank (www.rcsb.org) with the following accession codes: 6WZA (Ni^{II}:TriCyt1$_3$), 6X8X (Cu^{II}:TriCyt1$_3$), 6WYU (TriCyt2$_3$), 6WZ0 (Fe^{II}:TriCyt2$_3$), 6WZ1 (Mn^{II}:TriCyt3$_3$), 6WZ2 (Co^{II}:TriCyt3$_3$, Λ isomer), 6X7E (Co^{II}:TriCyt3$_3$, Δ isomer), 6WZC (Ni^{II}:TriCyt3$_3$), and 6WZ3 (Cu^{II}:TriCyt3$_3$).

References

[1]. a)Waldron KJ, Rutherford JC, Ford D, Robinson NJ, Nature 2009, 460, 823–830; [PubMed: 19675642] b)Williams RJP, J. Chem. Soc., Dalton Trans 1991, 539−546;c)Frausto da Silva JJR, Williams RJP, The biological chemistry of the elements, Oxford University Press, Oxford, 2001.

[2]. a)Cook SA, Hill EA, Borovik AS, Biochemistry 2015, 54, 4167–4180; [PubMed: 26079379] b)Churchfield Lewis A., George A, Tezcan FA, Essays in Biochem 2017, 61, 245–258; [PubMed: 28487401] c)Nastri F, D'Alonzo D, Leone L, Zambrano G, Pavone V, Lombardi A, Trends in Biochem. Sci 2019.

[3]. a)Bertini I, Gray HB, Stiefel EI, Valentine JS, Biological Inorganic Chemistry, Structure & Reactivity, University Science Books, Sausalito, 2007;b)Lippard S, Berg J, Principles of Bioinorganic Chemistry, University Science Books, Mill Valley, 1994;c)Holm RH, Kennepohl P, Solomon EI, Chem. Rev 1996, 96, 2239–2314; [PubMed: 11848828] d)Holm RH, Solomon EI, 2014, 114, 3367–3368.

[4]. a)Lu Y, Yeung N, Sieracki N, Marshall NM, Nature 2009, 460, 855–862; [PubMed: 19675646] b)Yu F, Cangelosi VM, Zastrow ML, Tegoni M, Plegaria JS, Tebo AG, Mocny CS, Ruckthong L, Qayyum H, Pecoraro VL, Chem. Rev 2014, 114, 3495–3578; [PubMed: 24661096] c)Schwizer F, Okamoto Y, Heinisch T, Gu Y, Pellizzoni MM, Lebrun V, Reuter R, Köhler V, Lewis JC, Ward TR, Chem. Rev 2018, 118, 142–231. [PubMed: 28714313]

[5]. a)Handel TM, Williams SA, Degrado WF, Science 1993, 261, 879–885; [PubMed: 8346440] b)DeGrado WF, Summa CM, Pavone V, Nastri F, Lombardi A, Annu. Rev. Biochem 1999, 68, 779–819. [PubMed: 10872466]

[6]. a)Faiella M, Andreozzi C, de Rosales RTM, Pavone V, Maglio O, Nastri F, DeGrado WF, Lombardi A, Nat. Chem. Biol 2009, 5, 882–884; [PubMed: 19915535] b)Reig AJ, Pires MM, Snyder RA, Wu Y, Jo H, Kulp DW, Butch SE, Calhoun JR, Szyperski T, Solomon EI, DeGrado WF, Nat. Chem 2012, 4, 900; [PubMed: 23089864] c)Joh NH, Wang T, Bhate MP, Acharya R, Wu Y, Grabe M, Hong M, Grigoryan G, DeGrado WF, Science 2014, 346, 1520–1524; [PubMed: 25525248] d)Ghirlanda G, Osyczka A, Liu WX, Antolovich M, Smith KM, Dutton PL, Wand AJ, DeGrado WF, J. Am. Chem. Soc 2004, 126, 8141–8147; [PubMed: 15225055] e)Roy A, Sommer DJ, Schmitz RA, Brown CL, Gust D, Astashkin A, Ghirlanda G, J. Am. Chem. Soc 2014, 136, 17343–17349; [PubMed: 25437708] f)Nanda V, Rosenblatt MM, Osyczka A, Kono H, Getahun Z, Dutton PL, Saven JG, DeGrado WF, J. Am. Chem. Soc 2005, 127, 5804–5805; [PubMed: 15839675] g)Mutter AC, Tyryshkin AM, Campbell IJ, Poudel S, Bennett GN, Silberg JJ, Nanda V, Falkowski PG, Proc. Natl. Acad. Sci. USA 2019, 116, 14557–14562; [PubMed: 31262814]

h)Shifman JM, Gibney BR, Sharp RE, Dutton PL, Biochemistry 2000, 39, 14813–14821; [PubMed: 11101297] i)Robertson DE, Farid RS, Moser CC, Urbauer JL, Mulholland SE, Pidikiti R, Lear JD, Wand AJ, DeGrado WF, Dutton PL, Nature 1994, 368, 425–432; [PubMed: 8133888] j)Koder RL, Anderson JLR, Solomon LA, Reddy KS, Moser CC, Dutton PL, Nature 2009, 458, 305–309; [PubMed: 19295603] k)Bender GM, Lehmann A, Zou H, Cheng H, Fry HC, Engel D, Therien MJ, Blasie JK, Roder H, Saven JG, DeGrado WF, J. Am. Chem. Soc 2007, 129, 10732–10740; [PubMed: 17691729] l)Zastrow ML, Pecoraro VL, Biochemistry 2014, 53, 957–978; [PubMed: 24506795] m)Matzapetakis M, Pecoraro VL, J. Am. Chem. Soc 2005, 127, 18229–18233; [PubMed: 16366576] n)Tegoni M, Yu F, Bersellini M, Penner-Hahn JE, Pecoraro VL, Proc. Natl. Acad. Sci. USA 2012, 109, 21234–21239; [PubMed: 23236170] o)Tolbert AE, Ervin CS, Ruckthong L, Paul TJ, Jayasinghe-Arachchige VM, Neupane KP, Stuckey JA, Prabhakar R, Pecoraro VL, Nat. Chem 2020, 12, 405–411; [PubMed: 32123337] p)Zhang S-Q, Chino M, Liu L, Tang Y, Hu X, DeGrado WF, Lombardi A, J. Am. Chem. Soc 2018, 140, 1294–1304; [PubMed: 29249157] q)Nanda V, Senn S, Pike DH, Rodriguez-Granillo A, Hansen WA, Khare SD, Noy D, Biochim. Biophys. Acta A 2016, 1857, 531–538;r)Ulas G, Lemmin T, Wu Y, Gassner GT, DeGrado WF, Nat. Chem 2016, 8, 354–359; [PubMed: 27001731] s)Berwick MR, Lewis DJ, Jones AW, Parslow RA, Dafforn TR, Cooper HJ, Wilkie J, Pikramenou Z, Britton MM, Peacock AFA, J. Am. Chem. Soc 2014, 136, 1166–1169. [PubMed: 24405157]

[7]. a)Lombardi A, Pirro F, Maglio O, Chino M, DeGrado WF, Acc. Chem. Res 2019, 52, 1148–1159; [PubMed: 30973707] b)Tebo AG, Pecoraro VL, Curr. Opin. Chem. Biol 2015, 25, 65–70; [PubMed: 25579452] c)Chino M, Leone L, Maglio O, D'Alonzo D, Pirro F, Pavone V, Nastri F, Lombardi A, Angew. Chem., Int. Ed 2017, 56, 15580–15583;d)Stenner R, Steventon JW, Seddon A, Anderson JLR, Proc. Natl. Acad. Sci. U.S.A, 2020, 117, 1419–1428. [PubMed: 31896585]

[8]. a)Eck RV, Dayhoff MO, Science 1966, 152, 363–366; [PubMed: 17775169] b)Armstrong RN, Biochemistry 2000, 39, 13625–13632; [PubMed: 11076500] c)Bergdoll M, Eltis LD, Cameron AD, Dumas P, Bolin JT, Prot. Sci 1998, 7, 1661–1670.

[9]. a)Salgado EN, Ambroggio XI, Brodin JD, Lewis RA, Kuhlman B, Tezcan FA, Proc. Natl. Acad. Sci. USA 2010, 107, 1827–1832; [PubMed: 20080561] b)Salgado EN, Radford RJ, Tezcan FA, Acc. Chem. Res 2010, 43, 661–672; [PubMed: 20192262] c)Churchfield LA, Tezcan FA, Acc. Chem. Res 2019, 52, 345–355. [PubMed: 30698941]

[10]. Faraone-Mennella J, Tezcan FA, Gray HB, Winkler JR, Biochemistry 2006, 45, 10504–10511. [PubMed: 16939202]

[11]. Salgado EN, Faraone-Mennella J, Tezcan FA, J. Am. Chem. Soc 2007, 129, 13374–13375. [PubMed: 17929927]

[12]. a)Salgado EN, Lewis RA, Faraone-Mennella J, Tezcan FA, J. Am. Chem. Soc 2008, 130, 6082–6084; [PubMed: 18422313] b)Salgado EN, Lewis RA, Mossin S, Rheingold AL, Tezcan FA, Inorg. Chem 2009, 48, 2726–2728. [PubMed: 19267481]

[13]. a)Medina-Morales A, Perez A, Brodin JD, Tezcan FA, J. Am. Chem. Soc 2013, 135, 12013–12022; [PubMed: 23905754] b)Salgado EN, Brodin JD, To MM, Tezcan FA, Inorg. Chem 2011, 50, 6323–6329; [PubMed: 21648390] c)Brodin JD, Medina-Morales A, Ni T, Salgado EN, Ambroggio XI, Tezcan FA, J. Am. Chem. Soc 2010, 132, 8610–8617. [PubMed: 20515031]

[14]. a)Churchfield LA, Medina-Morales A, Brodin JD, Perez A, Tezcan FA, J. Am. Chem. Soc 2016, 138, 13163–13166; [PubMed: 27649076] b)Churchfield LA, Alberstein RG, Williamson LM, Tezcan FA, J. Am. Chem. Soc 2018, 140, 10043–10053. [PubMed: 29996654]

[15]. a)Song WJ, Tezcan FA, Science 2014, 346, 1525–1528; [PubMed: 25525249] b)Song WJ, Yu J, Tezcan FA, J. Am. Chem. Soc 2017, 139, 16772–16779. [PubMed: 28992705]

[16]. a)Fink AL, Fold. Des 1998, 3, R9–R23; [PubMed: 9502314] b)Garcia-Seisdedos H, Empereur-Mot C, Elad N, Levy ED, Nature 2017, 548, 244–247. [PubMed: 28783726]

[17]. Irving H, Williams RJP, Nature 1948, 162, 746–747.

[18]. a)Gagnon DM, Brophy MB, Bowman SEJ, Stich TA, Drennan CL, Britt RD, Nolan EM, J. Am. Chem. Soc 2015, 137, 3004–3016; [PubMed: 25597447] b)Hayden JA, Brophy MB, Cunden LS, Nolan EM, J. Am. Chem. Soc 2013, 135, 775–787. [PubMed: 23276281]

[19]. Zygiel EM, Nolan EM, Annu. Rev. Biochem 2018, 87, 621–643. [PubMed: 29925260]

[20]. Grynkiewicz G, Poenie M, Tsien RY, J. Biol. Chem 1985, 260, 3440–3450. [PubMed: 3838314]

[21]. Golynskiy MV, Gunderson WA, Hendrich MP, Cohen SM, Biochemistry 2006, 45, 15359–15372. [PubMed: 17176058]

[22]. Rittle J, Field MJ, Green MT, Tezcan FA, Nat. Chem 2019, 11, 434–441. [PubMed: 30778140]

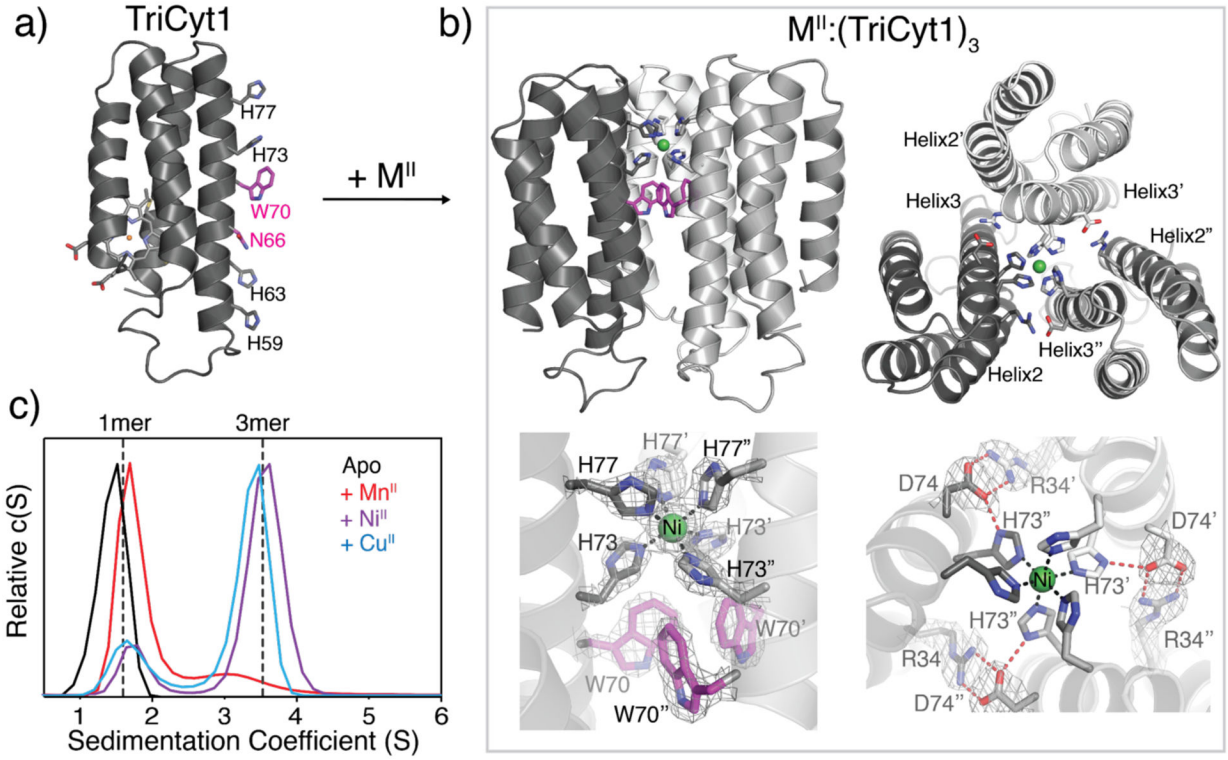

Figure 1.

A) Structural model of TriCyt1 monomer. B) Crystal structure of the Ni^{II}:$(TriCyt1)_3$ trimer (PDB ID: 6WZA), which is essentially identical to that of Cu^{II}:$(TriCyt1)_3$ (Figure S2, PDB ID: 6X8X). The upper panels show the side- and top-views of the trimer and the bottom panels depict the primary and secondary coordination environments that comprise the "core motif". The 2*F*o–*F*c maps (grey mesh) are contoured at 1σ. C) Sedimentation velocity (SV) profiles of TriCyt1 (30 μM monomer) in the absence and presence of 10 μM $MnCl_2$, $NiCl_2$, and $CuCl_2$ (see Figure S4 for a complete set).

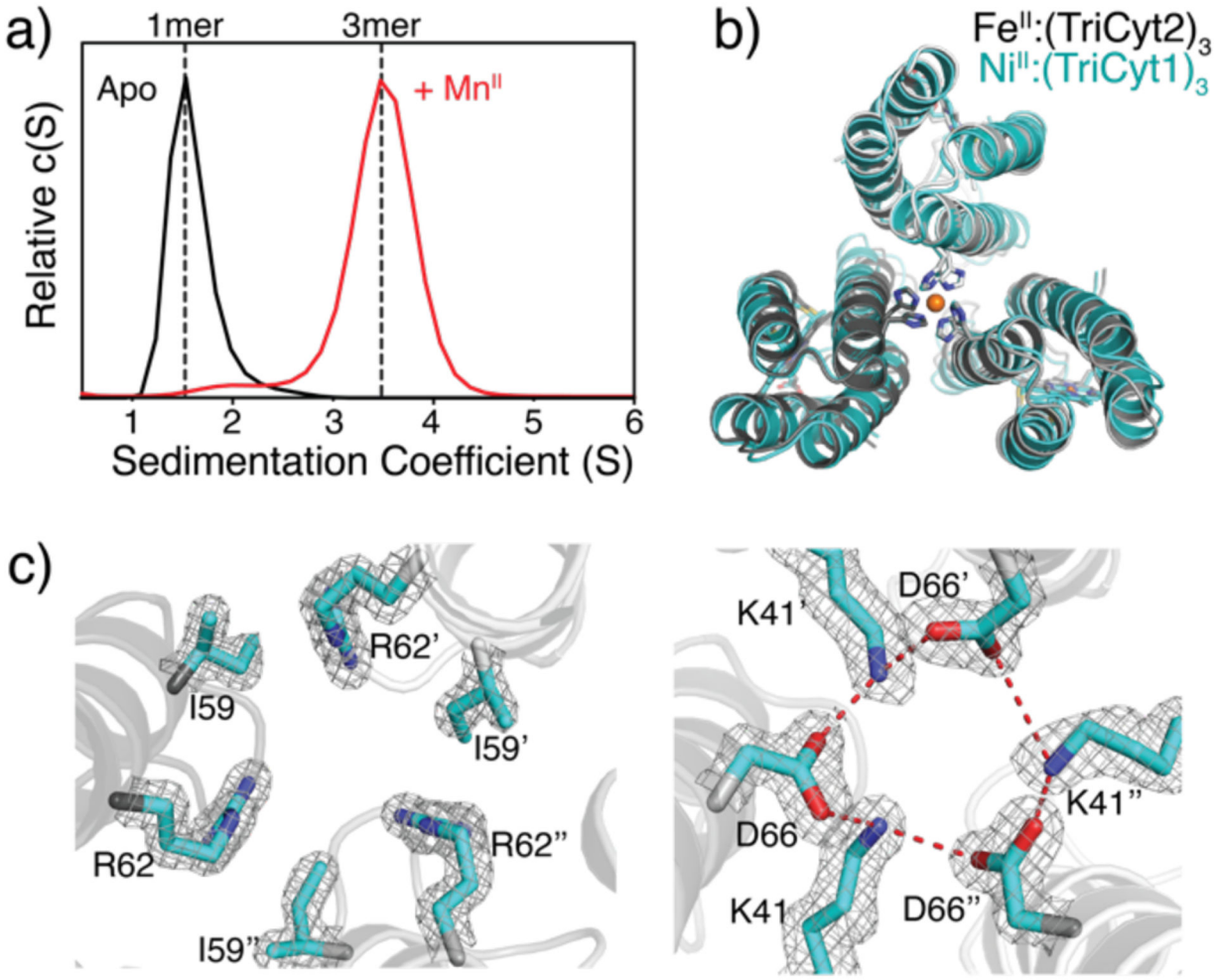

Figure 2.

A) SV profiles of TriCyt2 (30 μM monomer) in the absence and presence of 10 μM $MnCl_2$. B) Structural overlay of Fe^{II}:$(TriCyt2)_3$ (grey, PDB ID: 6WZ0) and Ni^{II}:$(TriCyt1)_3$ (cyan, PDB ID: 6WZA). C) Hydrophobic packing (left) and H-bonding (right) interactions at the core interface of Fe^{II}:$(TriCyt2)_3$. The 2*F*o–*F*c maps (grey mesh) are contoured at 1σ.

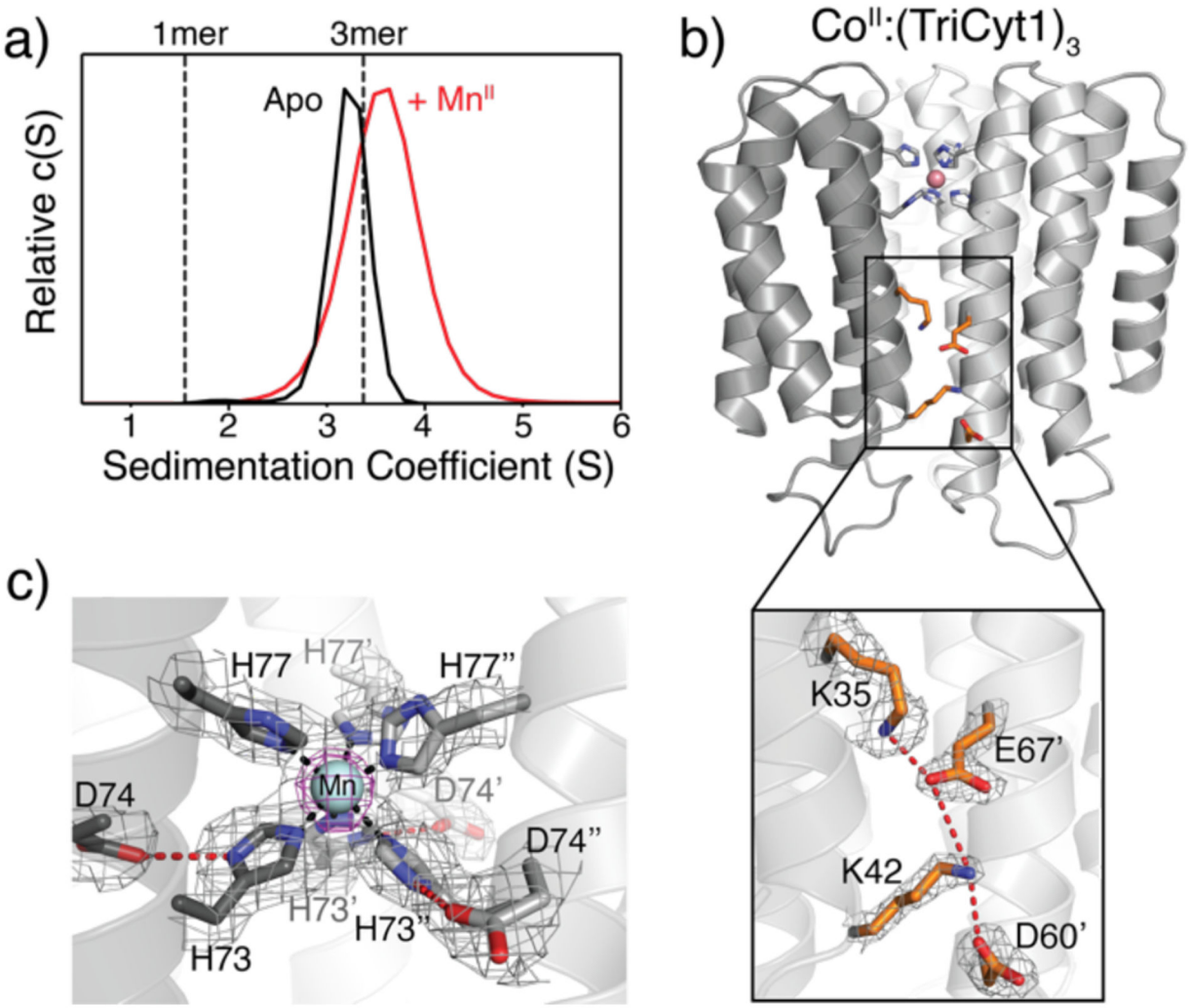

Figure 3.

A) SV profiles of TriCyt3 in the absence and presence of $MnCl_2$. B) Crystal structure of Co^{II}:$(TriCyt3)_3$ (PDB ID: 6WZ2), highlighting engineered H-bonding/electrostatic interactions in peripheral interfaces. C) His_6-Mn^{II} coordination environment in Mn^{II}:$(TriCyt3)_3$ (PDB ID: 6WZ1). The 2*F*o–*F*c (grey) and Mn^{II}-anomalous difference (purple) maps are contoured at 1σ and 5σ, respectively.

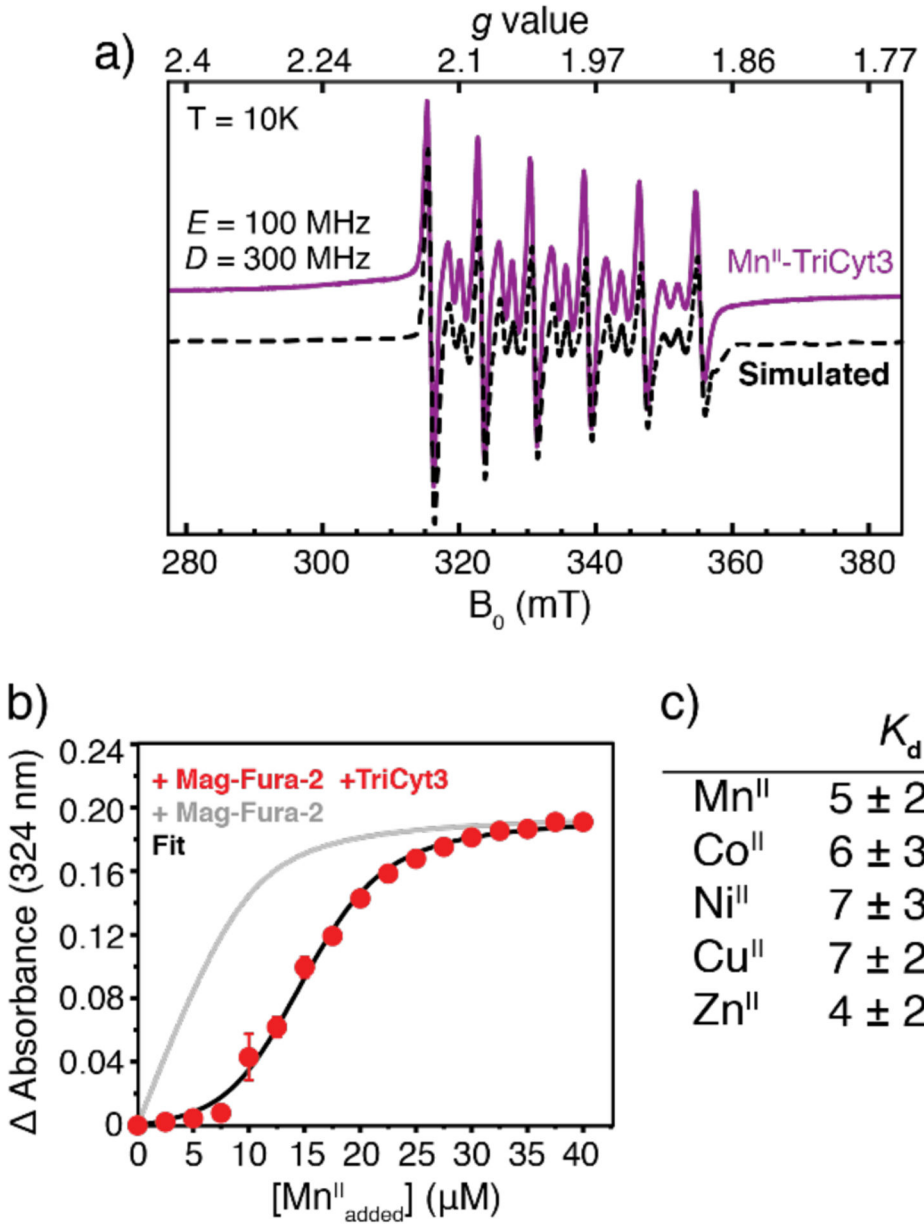

Figure 4.

A) X-band EPR spectrum of Mn^{II}:$(TriCyt3)_3$. B) Mn^{II}-binding isotherm for competitive binding titration of TriCyt3 in the presence of Mag-Fura-2. C) Dissociation constants for M^{II}:$(TriCyt3)_3$ complexes determined by competition titrations (see also Figures S14 and S15, and Tables S7 and S8). Metal was added in 2.5 μM increments from 2.5 mM metal chloride stock solutions. The standard errors shown are the standard errors of the fits as calculated by the data fitting program DynaFit (see Supporting Materials and Methods section of the SI).